An Ultraviolet Fiber Fabry–Pérot Cavity for Florescence Collection of Trapped Ions *

Kun Zhou(周坤)[1,2†], Jin-Ming Cui(崔金明)[1,2†], Yun-Feng Huang(黄运锋)[1,2**], Zhao Wang(王钊)[1,2], Zhong-Hua Qian(钱忠华)[1,2], Qi-Ming Wu(伍启明)[1,2], Jian Wang(王健)[1,2], Ran He(贺冉)[1,2], Wei-Min Lv(吕为民)[1,2], Chang-Kang Hu(胡长康)[1,2], Yong-Jian Han(韩永建)[1,2**], Chuan-Feng Li(李传锋)[1,2**], Guang-Can Guo(郭光灿)[1,2]

[1]*Key Laboratory of Quantum Information, University of Science and Technology of China, Chinese Academy of Sciences, Hefei 230026*

[2]*Synergetic Innovation Center of Quantum Information and Quantum Physics, University of Science and Technology of China, Hefei 230026*

(Received 13 September 2016)

We demonstrate a fiber Fabry–Pérot cavity in the ultraviolet range, which covers the florescence wavelength for the $^2P_{1/2}$ to $^2S_{1/2}$ transition of Yb^+ and is designed in the bad cavity limit for florescence collection. Benefiting from both the small cavity mode volume and the large atom dipole, a cavity with moderate finesse and high transmission still supports a good cooperativity, which is made and tested in experiment. Based on the measured experimental parameters, simulation performed on the cavity and ion shows a Purcell factor better than 2.5 and a single-mode fiber collection efficiency over 10%. This technology can support ultra-bright single photon sources based on trapped ions and can provide the possibility to link remote atoms as a quantum network.

PACS: 37.30.+i, 42.50.Pq, 42.81.Wg DOI: 10.1088/0256-307X/34/1/013701

A Fabry–Pérot optical micro-cavity, which is based on concave mirrors on fiber-end faces, combines advantages of small mode volume, high finesse, open access, and direct fiber mode coupling ability.[1] It provides powerful applications in many fields, such as cold atoms,[2] diamond photonics,[3] Raman enhancement,[4] and trapped ions.[5–7] Benefiting from the large coupling factor between a single photon and a single dipole emitter, the Purcell enhancement on spontaneous emission, or even strong coupling can be reached in cavity quantum electrodynamics (CQED).

Trapped ions have both solid-state-like stable trapping ability and high spectrum purity. More importantly, they can be trapped in the Lamb–Dick regime, which offers an ideal platform for demonstrating quantum information processing (QIP), such as quantum simulation,[8] quantum communication,[9] and quantum computation.[10] However, it is still a large challenge to build a large-scale quantum computer and long-distance quantum communication. To implement such quantum tasks, the key ingredient is to remotely distribute entanglement efficiently.

There are two main schemes to remotely distribute entanglement between ions and both of them are using photons to propagate remotely.[11] One scheme is transferring the state of an ion to a photon, then the photon propagates and interacts with the remote ion.[12,13] In this scheme,[14] the interaction between the photon and the ion should be in strong coupling regime, and the atom should absorb the single photon with a high efficiency, which is difficult from the current technology. In the other scheme, a photon radiated from spontaneous emission is entangled with the ion itself; if we perform Bell state measurements on two emitted photons (each from one ion), the two ions can be deterministically entangled. This method does not require the strong coupling condition like quantum state transfer scheme,[12] and is robust with a high fidelity.[14] Therefore, this scheme is relatively more feasible to build large-scale modular quantum-computer architecture.[15,16] However, the efficiency of this scheme is still limited by the low single-mode fiber florescence collection efficiency for two-photon interference. Although many efforts have been made to improve it,[17–20] the reported coupling efficiency to a single optical fiber mode is about 1% in the current entanglement experiment.[21]

When a CQED system is in bad cavity limit, the Purcell enhancement offers a high ratio of emitting photons into cavity mode, which can enhance photon emission rate and photon collection efficiency simultaneously. An ion-trap integrated with an optical cavity at millimeter scale has been tried with this idea,[22] while the collection efficiency and photon counting rate are not significantly improved because of the poor

*Supported by the National Natural Science Foundation of China under Grant Nos 11274289, 11325419, 11474267, 11404319, 61327901, 61225025 and 11474268, the Fundamental Research Funds for the Central Universities under Grant Nos WK2470000018 and WK2030020019, the Strategic Priority Research Program (B) of the Chinese Academy of Sciences under Grant No XDB01030300, the National Youth Top Talent Support Program of National High-level Personnel of Special Support Program under Grant No BB2470000005, and the Anhui Provincial Natural Science Foundation under Grant No 1608085QA22.

† They contributed equally to this work.

**Corresponding author. Email: hyf@ustc.edu.cn; smhan@ustc.edu.cn; cfli@ustc.edu.cn

© 2017 Chinese Physical Society and IOP Publishing Ltd

cooperative factor of this system. As a fiber Fabry–Pérot cavity (FFPC) can provide a large Purcell factor, it has the potential to solve this problem. In addition, benefiting from high coupling efficiency between the single fiber mode and the cavity mode, total coupling efficiency to a single optical fiber mode will be much improved, and the scalability on entanglement generation scheme can be solved.

In this Letter, we present an FFPC with a moderate finesse at 369 nm, which is designed in the bad cavity limit for florescence enhancement at the wavelength of $^2P_{1/2}$ to $^2S_{1/2}$ transition of Yb^+. The transition has relatively simple hyperfine ground states, which is suitable for the entanglement generation scheme.[14] After characterizing the FFPC transmission, we estimate a Purcell factor above 2.5 and a single-mode fiber florescence collection efficiency over 10%. Owing to its high efficiency and integration ability, the FFPC has a potential to entangle remote ions to build a large quantum system, which is the basis for constructing quantum network and developing distributed quantum computation.

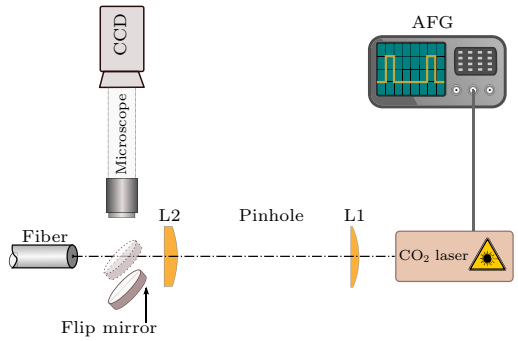

Fig. 1. Schematic diagram of laser machining setup for fabricating FFPCs. The pinhole is set on the focal plane of lens L1 as a spatial filter, L2 is an aspheric lens with a focal length of 50 mm, and the microscope is used to position the fiber core to the laser spot of L2 by the aid of the flip mirror.

Integrating FFPCs with trapped ions demands special design of the fiber cavity. One important thing is minimizing the impact of dielectric charging at fiber-end faces which can destabilize the trapped ions. In this case, a long cavity length is required, which corresponds to a large radius of curvature (ROC) of the mirror profile. Furthermore, to support polarization entanglement generation based on the Bell measurement,[15] both polarizations should resonate with the cavity mode, thus the birefringence splitting should be less than the line width of the cavity,[23] which demands a low eccentricity of the concave surface profile. To meet the above requirements, a laser machining setup is designed as shown in Fig. 1 to fabricate the concave mirror profile on the fiber-end faces. Different from the previously reported refined methods,[23,24] here we reduce the eccentricity by improving beam quality with spatial filtering. To improve the output beam quality of the CO_2 laser (Synrad Firestar v40), an aluminum pinhole is placed on the focal plane of lens L1 as a spatial filter. The diameter of the pinhole is set as 500 μm, which is below the diffraction-limited spot size of 570 μm. Higher order modes can be efficiently filtered out by the pinhole, and a more pure fundamental laser mode can be obtained, which means a better circularly symmetric laser power density distribution. An aspheric lens L2 (Thorlabs AL72550-G, $f = 50$ mm) focuses the filtered laser to the fiber-end face (Thorlabs SM300), the spot size on the fiber-end face can be changed from 60 μm to 250 μm by varying the distance between the fiber-end face and the beam waist plane. A microscope with long working distance objective is used to image and position the fiber-end face by the aid of a flip mirror with high repeatability (Newport 8892-K-M motorized flipper mount). The bare fiber is clamped in a v-groove which is installed on a three-axis microstage (Thorlabs MBT616D/M) to perform fine adjustment at nanometer scale. The optical resolution of the microscope is 1 μm and the repeatable resolution caused by the flip mirror is 500 nm, both above the parameters supporting an alignment precision below 2 μm. The CO_2 laser is controlled by an arbitrary function generator (AFG) by pulse-width modulation; a typical single laser pulse to make a concave profile on the fiber-end face is typically 10 ms duration with 2 W power.

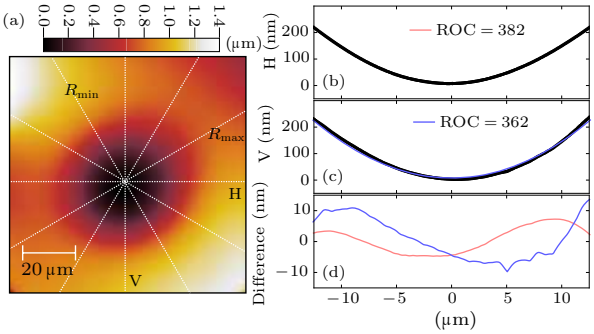

Fig. 2. Surface characterization of a typical machined fiber. (a) Mirror profile with an area of 90 μm×90 μm measured by an AFM. (b, c) Horizontal (H) and vertical (V) section of the dashed square of (a), black: section data, red (blue): circle fit of H (V). (d) Difference between data and fit in (b) and (c).

Following the laser machining process, we characterize the machined fiber-end surface profiles with an atomic force microscopy (AFM, Bruker Demension Icon). A typical measured surface profile data with an area of 90 μm × 90 μm is shown in Fig. 2(a). To measure the ROCs of the profile, sections are cut out along the H and V directions and presented as black lines in Figs. 2(b) and 2(c). A circle formula $(y = y_0 + \sqrt{\mathrm{ROC}^2 - (x - x_0)^2})$ is used to fit the section data, and the fits are shown as the red line in Fig. 2(b) and blue line in Fig. 2(c), respectively. The corresponding differences between the data and their fits are plotted in Fig. 2(d), which shows that all of the differences are under 15 nm. To balance the cavity length and mode volume, the cavity length is set

between 100 μm and 300 μm. In this case, the diameter of the fundamental mode waist on the cavity mirrors will be less than 6 μm; it is much less than 25 μm range analyzed in Fig. 2(d), thus the clipping loss of the cavity can be ignored.[1] Figure 2(a) shows an elliptical surface profile, and the eccentricity can be calculated as $\varepsilon = \sqrt{1 - R_{\rm min}/R_{\rm max}}$, where $R_{\rm min}$ and $R_{\rm max}$ are the estimated ROCs along the minor and major axes of the profile selected from the six sections seen in Fig. 2(a). With this method, we find an averaged eccentricity of 0.22 ± 0.04 on 24 samples with ROCs ranging from 150 μm to 450 μm, which is in the same level as the optimized laser machining with circular polarization.[23]

After successful machining, the concave mirrors are coated for high reflection in ultraviolet range by ion-beam sputtering. The coating is designed with a moderate transmission $T = 0.19\%$ at 369 nm. Then, two coated fibers are aligned as shown in the inset of Fig. 3(a) to form the microcavity, where one fiber is clamped on a 6-axis nano-stage (Thorlabs MAX603D/M) for alignment, and the other fiber is installed on a piezo (PI-E753) to scan the cavity length. A 369 nm laser from a Toptica SHG pro is coupled into one of the fibers, passing through the cavity to the other fiber, and finally detected by a 125 MHz photo-receiver (New Port: 1801-FC-AC). Transmission spectrum of the cavity is measured by scanning the cavity length, a typical transmission spectrum is shown in Fig. 3(a), which contains four resonant peaks of fundamental modes and the second peak is magnified in Fig. 3(b). By measuring multiple peak widths and distances, the finesse $\mathcal{F}$ is acquired as 1300 ± 100. From $\mathcal{F} = \pi/(1-R)$, we can deduce that the reflection of the coating is $R = 99.76\%$ and the loss of the coating is $\mathcal{L} = 1 - R - T = 0.05\%$.

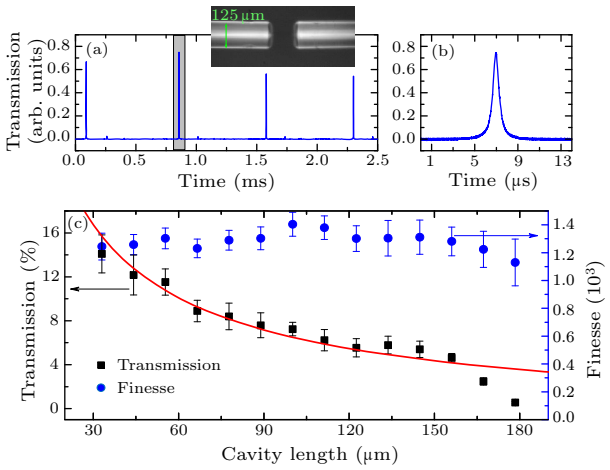

Fig. 3. Transmission measurement of the FFPC. (a) Transmission spectrum at 369 nm by scanning the cavity length over three free spectrum ranges. Inset: the cavity configuration. (b) Details of the second peak in (a). (c) The cavity finesse (blue dots) and total transmission efficiency (black cubes) versus the cavity lengths, and the red line is the simulated total transmission efficiency.

In the bad cavity limit, the florescence collection efficiency from a trapped ion in an FFPC into the single-mode fiber is

$$\eta = \eta_{\rm m} \cdot \eta_{\rm t} \cdot \eta_{\rm c} = \frac{C_0}{1 + C_0} \cdot \frac{T}{1 - R} \cdot \eta_{\rm c}, \qquad (1)$$

where $\eta_{\rm m}$ is the coupling efficiency from a trapped ion to the cavity mode, C_0 is the single-atom cooperative factor which determines the Purcell factor, $\eta_{\rm t}$ is the transmission efficiency of the coating on fiber-end faces when the cavity is resonant, and $\eta_{\rm c}$ is the mode coupling efficiency between the cavity mode and the fiber mode, which can be expressed as[1]

$$\eta_{\rm c} = 4/\left[\left(\frac{\omega_{\rm f}}{\omega_{\rm m}} + \frac{\omega_{\rm m}}{\omega_{\rm f}}\right)^2 + \left(\frac{\pi n_{\rm f} \omega_{\rm f} \omega_{\rm m}}{\lambda \cdot {\rm ROC}}\right)^2\right], \qquad (2)$$

where $\omega_{\rm m}$ is the cavity mode radius on cavity mirrors, $\omega_{\rm f}$ is the fiber mode radius, and $n_{\rm f}$ is the refractive index of the fiber. By measuring the total light transmission efficiency of the FFPC, which is $\eta_{\rm tt} = \eta_{\rm c}\eta_{\rm t}\eta_{\rm t}\eta_{\rm c}$, the florescence transmission from a trapped ion in the cavity to the fiber mode can be determined as $\eta_{\rm t} \cdot \eta_{\rm c} = \sqrt{\eta_{tt}}$. Figure 3(c) presents the total transmission efficiency (black squares) and the finesse (blue dots) of the FFPC versus the cavity length, which clearly shows that the transmission efficiency decreases while increasing the cavity length. In contrast, the finesse is constant if the measurement noise is ignored. A simulated transmission efficiency line is shown as a red line, which is in accordance with the measured data corresponding to the cavity lengths shorter than 160 μm. In this range, the total transmission is above 4%, which provides $\eta_{\rm t}\eta_{\rm c} > 20\%$. Here $\eta_{\rm tt}$ drops greatly with cavity lengths longer than 160 μm. This may come from the fundamental mode deficiencies caused by transverse-mode coupling.[25]

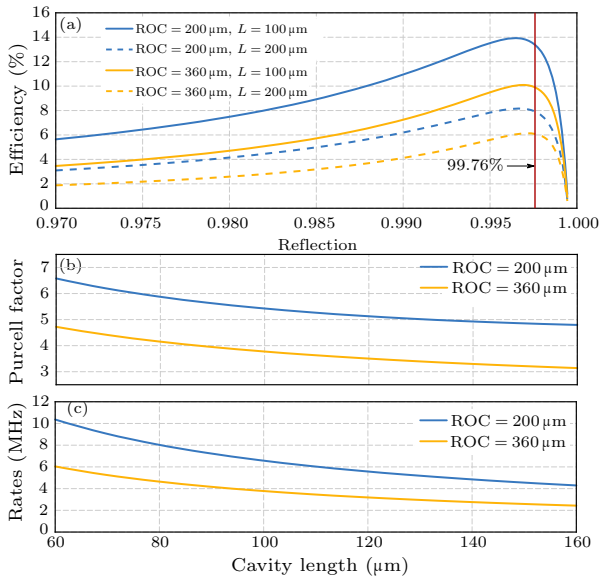

Fig. 4. Numerical simulation of the florescence enhancement of a trapped Yb^+ with an FFPC. Two cavities with ROC=360 μm (yellow lines) and ROC=200 μm (blue lines) are simulated. (a) Collection efficiency with the reflection of the output mirror. (b, c) The Purcell enhancement factor and photon emission rates into single fiber modes of FFPCs along with cavity length.

If both the mirrors have the same transmittance, florescence of the trapped ion will be coupled into the two fibers in different directions, which will complicate the entanglement generation using the Bell measurement. Thus an FFPC with a single output port should be used in future experiments. To make up a single output cavity with the previous $T = 0.19\%$ fiber mirror, another coated fiber mirror with much lower transmittance is prepared with parameters $T' = 0.01\%$, $R' = 99.93\%$ and $\mathcal{L}' = 0.06\%$. As the cooperative factor C_0 with a trapped Yb^+ can be calculated from the cavity finesse and length

$$C_0 = \frac{g_0^2}{2\kappa\gamma_\perp} = \frac{3\lambda^2 c\gamma_0}{8\pi V_{\rm m}} \cdot \frac{1}{\kappa\gamma_0} = \frac{6\lambda}{\pi^2}\frac{\mathcal{F}}{\sqrt{2{\rm ROC}\cdot L - L^2}}, \quad (3)$$

where γ_0 is the spontaneous emission rate, κ is the electrical decay rate, $V_{\rm m}$ is the cavity mode volume, and $\gamma_\perp$ is the overall dipole decay rate. For a trapped ion in ultrahigh vacuum, the atom is only radiatively broadened, thus $\gamma_\perp = \gamma_0/2$. We can simulate the single-mode fiber florescence collection efficiency from the coating parameters by combining with the simulated total transmission efficiency in Fig. 3(c). The simulation results of two cavities with different ROCs are depicted in Fig. 4, where blue and yellow lines are used for the cavities with ROCs of 200 μm and 360 μm, respectively. Figure 4(a) shows the single-mode fiber Yb^+ florescence collection efficiency versus the reflection of the cavity output mirror, and the red line is the reflection of the coatings in the experiment. As smaller mode volumes of short cavities support larger cooperative factors, they provide better performance, as well as the cavities with smaller ROCs. An efficiency over 10% can be obtained with the cavity length of 100 μm and the mirror ROC of 200 μm. The Purcell enhancement ($F_{\rm p} = 2C_0$) versus the cavity length is presented in Fig. 4(b). It shows that a factor above 2.5 can be reached in experiment. Figure 4(c) gives the maximum photon emission rates into the single fiber mode with continuous pumping condition. An output with several megahertz photon rates indicates that this is an ultrabright single-photon source.

In summary, we have demonstrated an FFPC with ultraviolet wavelength and presented the analysis in enhancing and collecting the florescence of a trapped ion. We take the Yb^+ ion as an example for simulation. As a single ion has already been trapped in a needle trap with a similar FFPC,[26] future experiments integrating our FFPC with trapped ions can be demonstrated without any obstacle. Furthermore, our scheme can be applied to most trapped ion species in current experiment just by modifying the coating of the mirrors. Compared with infrared cavities designed for $^2P_{1/2}$ to $^2D_{3/2}$ transition,[5–7] the ultraviolet cavities designed for $^2P_{1/2}$ to $^2S_{1/2}$ transition have much lesser branching ratios and support high emission rates, which are rather suitable for measurement based entanglement generation. By the aid of the FFPC in this work, polarization entanglement generation rate will exceed hundreds of Hertz, which makes the entanglement generation time much less than the coherent time of ions.

References

[1] Hunger D, Steinmetz T, Colombe Y, Deutsch C, Hänsch T W and Reichel J 2010 *New J. Phys.* **12** 065038
[2] Colombe Y, Steinmetz T, Dubois G, Linke F, Hunger D and Reichel J 2007 *Nature* **450** 272
[3] Kaupp H, Deutsch C, Chang H C, Reichel J, Hänsch T W and Hunger D 2013 *Phys. Rev.* A **88** 053812
[4] Petrak B, Djeu N and Muller A 2014 *Phys. Rev.* A **89** 023811
[5] Brandstätter B et al 2013 *Rev. Sci. Instrum.* **84** 123104
[6] Steiner M, Meyer H M, Reichel J and Köhl M 2014 *Phys. Rev. Lett.* **113** 263003
[7] Meyer H M et al 2015 *Phys. Rev. Lett.* **114** 123001
[8] Blatt R and Roos C F 2012 *Nat. Phys.* **8** 277
[9] Duan L M and Monroe C 2010 *Rev. Mod. Phys.* **82** 1209
[10] Häffner H, Roos C F and Blatt R 2008 *Phys. Rep.* **469** 155
[11] Kimble H J 2008 *Nature* **453** 1023
[12] Russo C et al 2009 *Appl. Phys.* B **95** 205
[13] Reiserer A and Rempe G 2015 *Rev. Mod. Phys.* **87** 1379
[14] Moehring D L et al 2007 *Nature* **449** 68
[15] Monroe C and Kim J 2013 *Science* **339** 1164
[16] Monroe C et al 2014 *Phys. Rev.* A **89** 022317
[17] Maiwald R et al 2009 *Nat. Phys.* **5** 551
[18] Maiwald R 2012 *Phys. Rev.* A **86** 043431
[19] Takahashi et al 2013 *New J. Phys.* **15** 053011
[20] Jechow A, Streed E W, Norton B G, Petrasiunas M J and Kielpinski D 2011 *Opt. Lett.* **36** 1371
[21] Hucul D et al 2014 *Nat. Phys.* **11** 37
[22] Sterk J D, Luo L, Manning T A, Maunz P and Monroe C 2012 *Phys. Rev.* A **85** 062308
[23] Uphoff M, Brekenfeld M, Rempe G and Ritter S 2015 *New J. Phys.* **17** 013053
[24] Takahashi H, Morphew J, Oručević F, Noguchi A, Kassa E and Keller M 2014 *Opt. Express* **22** 31317
[25] Benedikter J, Hümmer T, Mader M, Schlederer B, Reichel J, Hänsch T W and Hunger D 2015 *New J. Phys.* **17** 053051
[26] Steiner M, Meyer H M, Deutsch C, Reichel J and Köhl M 2013 *Phys. Rev. Lett.* **110** 043003